

Application of positivity-preserving well-balanced discontinuous Galerkin method in computational hydrology



Xiao Wen^a, Zhen Gao^{a,*}, Wai Sun Don^a, Yulong Xing^b, Peng Li^c

^aSchool of Mathematical Sciences, Ocean University of China, Qingdao, China

^bDepartment of Mathematics, University of California at Riverside, California, USA

^cState Key Laboratory of Explosion Science and Technology, Beijing Institute of Technology, Beijing, China

ARTICLE INFO

Article history:

Received 31 October 2015

Revised 15 April 2016

Accepted 18 April 2016

Available online 19 April 2016

Keywords:

Discontinuous Galerkin

Positivity-preserving

Well-balanced

Shallow water equations

Tidal bores

ABSTRACT

The positivity-preserving well-balanced discontinuous Galerkin (DG) method (Xing et al. *J Sci Comput* **57**, 2013) is employed to solve the shallow water equations on an unstructured triangular mesh and to study their applications in computational hydrology. The grid convergence of the DG method is verified via the steady state oblique hydraulic jump problem. The dam-breaking problems with wet and dry river beds are conducted to demonstrate the positivity-preserving property of the scheme. The tidal bores in an idealized estuary problem are simulated to study the development and evolution of the tidal bores from different amplitudes of incoming tidal waves and topography of the river bed bottom. The numerical experiments above demonstrate that the DG method can be applied successfully to these class of problems in computational hydrology.

© 2016 Elsevier Ltd. All rights reserved.

1. Introduction

In the field of hydrology, there is a class of special flows in which the water level and velocity change rapidly and abruptly. In these flows, strong gradients or discontinuities often appear in the flows, for example, a sharp water level drop due to the discontinuities in the initial condition resulting from a breaking of a dam, and a development of sharp tidal bores due to the strong nonlinearity interaction between an outgoing river water and an incoming ocean tidal waves at the estuary. The tidal bores are a tidal phenomenon along a coast where a river empties into a sea in which the leading edge of the incoming high tide forms a wave (or waves) of water that travels up the river against the direction of the river current (also known as positive surge). However, there are only a few places, under some specific geological conditions, where the tidal bores can occur—not all coast features tidal bores. The river must be fairly shallow and has a narrow outlet to the sea. The estuary, the area where the river meets the sea, must be wide and flat. The coast's tidal wave length, the distance between high and low tides must be quite large (typically at least 6m). When all of these conditions are satisfied, a tidal bore is

formed. A few notable tidal bore systems in the world are the Pororoca Tidal Bore with Amazon river, Brazil, Bono Tidal Bore with Kampar River, Indonesia, Severn Tidal Bore with Severn River, United Kingdom, Silver Dragon Tidal Bore with Qiantang River, China and Turnagain Arm Tidal Bore with Cook Inlet, Alaska. An exception of the conditions above is the Amazon River where the mouth of the river is not narrow but shallow and dotted by many low-lying islands and sand bars. We refer the reader to the national geographic website¹ for more descriptions about the development and evolution of the tidal bores in the nature.

The research of the tidal bores has two basic goals. Academical-wise, the study of strong intermittent flow such as the tidal bores has been an important and challenging subject in hydrology. Research on the numerical simulations of tidal bores, not only can reveal the water dynamics of nonlinear wave laws, but also has an academic significance and a theoretical value in hydrodynamics and computational fluid dynamics. Engineering-wise, the study of the formation and evolution of the tidal bores, the in-depth understanding of its effect on estuarine environment and the effect of human activities on the tidal bores, can enhance the human survival and the economic and social development related to water environmental problems, preventing the potential harmful effects from the tidal bores while keeping this unique and valuable natural resource.

* Corresponding author. Tel.: +8613165072087.

E-mail addresses: xiaowen_ouc@163.com (X. Wen), zhengao@ouc.edu.cn (Z. Gao), waisundon@gmail.com (W.S. Don), xingy@ucr.edu (Y. Xing), weilailp@163.com (P. Li).

¹ <http://education.nationalgeographic.com/encyclopedia/tidal-bore/>

The shallow water equations serve as a very important model in the simulations of flows in the rivers, lakes and coastal areas, including the tidal bores. Although the shallow water equations have been studied extensively in the past two decades, they remain an active area of research in both theoretical studies and numerical simulations due to their practical importance. The traditional numerical methods for solving the shallow water equations are the method of characteristics (MOC), finite element method (FEM) and finite different Method (FDM). These methods have been successful in the simulations of many continuous flows, but are not satisfactory in solving discontinuous flows like the tidal bores. On one hand, one difficulty encountered in the simulation of shallow water equations is how to exactly balance the flux gradients by the source terms in the steady-state solution. The well-balanced schemes [1–6] are specially designed to preserve exactly the steady-state solution up to the machine error with relatively coarse meshes. Moreover, dry areas (where the water height is exactly equal to zero) might appear in the natural environments such as the dam-breaking problem over a dry river bed. Due to the Gibbs phenomenon when using a high order scheme without employing some forms of limiting on the solution and/or flux (limiter), a non-physical negative water height will be generated numerically in the simulations. It causes problem in calculating the eigenvalues that involve a square root of the water height. Therefore, many positivity-preserving schemes [7–11] were designed to preserve the positivity of certain physical quantities, such as the mass fraction in a reactive Euler equations and the water height in the shallow water equations with a dry area. A few of existing numerical methods [12–18] are able to maintain both the well-balance and positivity of the numerical schemes simultaneously.

Discontinuous Galerkin (DG) method is a class of finite element methods using discontinuous piecewise polynomial space as the solution and test function spaces (see [19] for a historic review and basic idea). It has been used extensively in solving the shallow water equations [20–26]. Recently, the positivity-preserving well-balanced DG method for the shallow water equations [16] was proposed to maintain the still water steady state solution exactly, and to preserve the non-negativity of the water height without a loss of mass conservation. In [17], a simple positivity-preserving limiter was extended to the DG method on the unstructured triangular meshes to guarantee the positivity of the water height.

In this study, we investigate the application of the positivity-preserving well-balanced DG method designed in [17] to the computational hydrology on the unstructured grids. We employ this method for simulating several challenging practical engineering problems such as the dam-breaking problems with wet and dry river beds and the development and evolution of the tidal bores in an idealized estuary. The grid convergence of the DG method is verified in the case of steady state oblique hydraulic jump. The positivity-preserving limiter is used in the DG method to avoid the non-physical negative water height in the simulations of dam-breaking problems with a dry river bed. The evolution of the flooding of the wet and dry river beds shows different flow structures that are unique in each individual case. A tidal bore is simulated to study the formation and evolution of the tidal bores with a trumpet-like shape river mouth emptying into an ocean while subjected to a large incoming tidal wave, similar to the one at the Qiantang River, China. We study factors like the tidal amplitude and river topography, which are related to the propagation and breaking of the undular tidal bores while moving up to the river against the current.

The paper is organized as follows. In Section 2, a very brief introduction to the positivity-preserving well-balanced DG method for the shallow water equations will be given. In Section 3, a classical two-dimensional steady state example is presented to validate the accuracy and convergence of the DG method. The

positivity-preserving well-balanced DG method is then applied to the dam-breaking problems with both wet and dry river beds. Also, an idealized estuary problem that simulates the formation and evolution of the tidal bores in a long straight river is shown. Finally, conclusion and future work are given in Section 4.

2. Positivity-preserving well-balanced DG method

The two-dimensional shallow water equations take the form

$$\begin{cases} h_t + (hu)_x + (hv)_y = 0 \\ (hu)_t + \left(hu^2 + \frac{1}{2}gh^2\right)_x + (huv)_y = -ghb_x \\ (hv)_t + (huv)_x + \left(hv^2 + \frac{1}{2}gh^2\right)_y = -ghb_y, \end{cases} \quad (1)$$

where h is the water height, $(u, v)^T$ is the velocity vector, $b(x, y)$ is the bottom topography and g is the gravitational constant. In a compact form, (1) can be written as

$$Q_t + \nabla \cdot \mathbf{F}(Q) = \mathbf{S}(h, b),$$

where $Q = (h, hu, hv)^T$ with the superscript T denoting the transpose, $\mathbf{F}(Q) = (f(Q), g(Q))$ is the flux vector and $\mathbf{S}(h, b)$ is the source term.

Let \mathcal{T}_τ be a family of triangular partitions of the computational domain Ω parameterized by $\tau > 0$. For any triangle $K \in \mathcal{T}_\tau$, we define $\tau_K := \text{diam}(K)$ and $\tau := \max_{K \in \mathcal{T}_\tau} \tau_K$. For each edge e_K^i ($i = 1, 2, 3$) of K , we denote its length by l_K^i , and outward unit normal vector by \mathbf{n}_K^i . Let $K(i)$ be the neighboring triangle along the edge e_K^i and $|K|$ be the area of the triangle K . In a high order DG method, we seek an approximation, still denoted by Q with an abuse of notation, which belongs to the finite dimensional space:

$$V_\tau = \{w \in L^2(\Omega); w|_K \in P^k(K) \ \forall K \in \mathcal{T}_\tau\}, \quad (2)$$

where $P^k(K)$ denotes the space of polynomials of degree at most k on K .

Let \mathbf{x} denotes (x, y) , the standard DG scheme is given by

$$\iint_K Q_t w \, d\mathbf{x} - \iint_K \mathbf{F}(Q) \cdot \nabla w \, d\mathbf{x} + \sum_{i=1}^3 \int_{e_K^i} \widehat{\mathbf{F}}|_{e_K^i} \cdot \mathbf{n}_K^i w \, ds = \iint_K \mathbf{S} w \, d\mathbf{x}, \quad (3)$$

where $w(\mathbf{x})$ is a test function, and the numerical flux $\widehat{\mathbf{F}}$ is defined by

$$\widehat{\mathbf{F}}|_{e_K^i} \cdot \mathbf{n}_K^i = \mathcal{F}(Q_i^{\text{int}(K)}, Q_i^{\text{ext}(K)}, \mathbf{n}_K^i), \quad (4)$$

where $Q_i^{\text{int}(K)}$ and $Q_i^{\text{ext}(K)}$ are the approximations to the values on the edge e_K^i obtained from the interior and the exterior of K . We could, for example, use the simple global Lax–Friedrichs flux

$$\mathcal{F}(a_1, a_2, \mathbf{n}) = \frac{1}{2}[\mathbf{F}(a_1) \cdot \mathbf{n} + \mathbf{F}(a_2) \cdot \mathbf{n} - \alpha(a_2 - a_1)],$$

where $\alpha = \max(|u| + \sqrt{gh}, |v| + \sqrt{gh})$ and the maximum is taken over the whole region. Notice that $h \geq 0$ should be a non-negative value at all time.

In order to achieve the well-balanced property, we are interested in preserving the still water stationary solution, namely,

$$h + b = \text{const}, \quad u = v = 0, \quad (5)$$

exactly. Well-balanced numerical methods are designed in [16,17], and take the form

$$\iint_K Q_t w \, d\mathbf{x} - \iint_K \mathbf{F}(Q) \cdot \nabla w \, d\mathbf{x} + \sum_{i=1}^3 \int_{e_K^i} \widehat{\mathbf{F}}^*|_{e_K^i} \cdot \mathbf{n}_K^i w \, ds = \iint_K \mathbf{S} w \, d\mathbf{x}, \quad (6)$$

where the well-balanced numerical fluxes $\widehat{\mathbf{F}}^*$ are given by

$$\widehat{\mathbf{F}}^*|_{e_K^i} \cdot \mathbf{n}_K^i = \mathcal{F}(Q_i^{*,\text{int}(K)}, Q_i^{*,\text{ext}(K)}, \mathbf{n}_K^i) + \langle \delta_{i,x}^*, \delta_{i,y}^* \rangle \cdot \mathbf{n}_K^i, \quad (7)$$

with the hydrostatic reconstruction

$$h_i^{*,int(K)} = \max(0, h_i^{int(K)} + b_i^{int(K)} - \max(b_i^{int(K)}, b_i^{ext(K)})),$$

$$h_i^{*,ext(K)} = \max(0, h_i^{ext(K)} + b_i^{ext(K)} - \max(b_i^{int(K)}, b_i^{ext(K)})), \quad (8)$$

and

$$Q_i^{*,int(K)} = \frac{h_i^{*,int(K)}}{h_i^{int(K)}} Q_i^{int(K)}, \quad \delta_{i,x}^* = \left(0, \frac{g}{2}(h_i^{int(K)})^2 - \frac{g}{2}(h_i^{*,int(K)})^2, 0\right)^T,$$

$$Q_i^{*,ext(K)} = \frac{h_i^{*,ext(K)}}{h_i^{ext(K)}} Q_i^{ext(K)}, \quad \delta_{i,y}^* = \left(0, 0, \frac{g}{2}(h_i^{int(K)})^2 - \frac{g}{2}(h_i^{*,int(K)})^2\right)^T, \quad (9)$$

on the edge e_k^i . More details of the well-balanced properties can be found in [17,27].

In order to obtain positivity-preserving property, we first introduce a special quadrature rule with the set of quadrature points denoted by S_K and weights w_x , satisfying: it is exact for integration of $h_K(\mathbf{x})$ on K ; it include all L -point Gauss quadrature points for each edge e_k^i ; and all the quadrature weights should be positive (see [17] for how to construct the quadrature rule and why these properties are useful). We would like to comment that this special quadrature rule is used only for the purpose of introducing the positivity-preserving limiters, and we can use any quadrature rule in computing the integral in (6). We then have the following results for the high order DG methods [17]:

Proposition 1. For the scheme (6) with a forward Euler time discretization to be positivity-preserving, i.e., $\bar{h}_K^{n+1} \geq 0$, a sufficient condition is that $h_K(\mathbf{x}) \geq 0, \forall \mathbf{x} \in S_K$ for all K , under the CFL condition:

$$\alpha \frac{\Delta t}{|K|} \sum_{i=1}^3 l_k^i \leq \frac{2}{3} \hat{w}_1. \quad (10)$$

Here $h_K(\mathbf{x})$ denotes the polynomial for the water height at time level n and the cell K , $\hat{w}_1 = 1/6$ ($k = 2, 3$) or $\hat{w}_1 = 1/12$ ($k = 4, 5$) is the quadrature weight of the M -point Gauss–Lobatto quadrature rule on $[-1/2, 1/2]$ for the first quadrature point.

At time level n , given the water height DG polynomial $h_K(\mathbf{x})$ with its cell average $\bar{h}_K^n \geq 0$, to enforce the sufficient condition $h_K(\mathbf{x}) \geq 0, \forall \mathbf{x} \in S_K$, the limiter in [16,17,28] can be used directly. The idea is to replace $h_K(\mathbf{x})$ by a linear scaling around the cell average:

$$\tilde{h}_K(\mathbf{x}) = \theta_K(h_K(\mathbf{x}) - \bar{h}_K^n) + \bar{h}_K^n, \quad (11)$$

where $\theta_K \in [0, 1]$ is determined by

$$\theta_K = \min_{\mathbf{x} \in S_K} \theta_{\mathbf{x}}, \quad \theta_{\mathbf{x}} = \min \left\{ 1, \frac{\bar{h}_K^n}{\bar{h}_K^n - h_K(\mathbf{x})} \right\}. \quad (12)$$

An alternative limiter is to enforce a relaxed condition, by replacing (12) with

$$\theta_K = \min \left\{ \theta_{\mathbf{x}^*}, \min_{\mathbf{x} \in \bar{S}_K} \theta_{\mathbf{x}} \right\}, \quad \theta_{\mathbf{x}} = \min \left\{ 1, \frac{\bar{h}_K^n}{\bar{h}_K^n - h_K(\mathbf{x})} \right\}, \quad (13)$$

to save time in evaluating θ_K . Here, we let \bar{S}_K and \tilde{S}_K be the set of points which lie in the interior and on the edges of triangle K , respectively. Since $\sum_{\mathbf{x} \in \bar{S}_K} h_K(\mathbf{x})w_x / \sum_{\mathbf{x} \in \bar{S}_K} w_x$ is a convex combination of point values of $h_K(\mathbf{x})$, thus by the Mean Value Theorem, there exists some point $\mathbf{x}^* \in K$ such that

$$h_K(\mathbf{x}^*) = \frac{1}{\sum_{\mathbf{x} \in \bar{S}_K} w_x} \sum_{\mathbf{x} \in \bar{S}_K} h_K(\mathbf{x})w_x,$$

which provides $\theta_{\mathbf{x}^*}$ in (13). Both limiters, (11) and (13), are conservative (the cell average of \tilde{h}_K is still \bar{h}_K^n) and high order accurate.

Table 1

The numerical solutions and the exact solution for the steady state oblique hydraulic jump problem.

τ_K (m)	N	α (°)	h (m)	u (m/s)
1.0	2683	30.8	1.495	7.895
0.5	10586	30.4	1.498	7.954
0.25	42104	30.1	1.499	7.957
Exact solution		30.0	1.500	7.956

When applied to problems containing discontinuous solution, DG methods may generate oscillation and even nonlinear instability. TVB limiters [29] are often applied to control these oscillations. For time discretization, the third order TVD Runge–Kutta scheme is used. The CFL = 1/3 and $k = 2$ are used in the following numerical examples. In the numerical experiments in the next section, the unstructured triangular meshes are generated by Easymesh².

3. Numerical experiments

In this section, we perform the positivity-preserving well-balanced DG method to simulate several challenging problems such as the oblique hydraulic jump problem, the dam-breaking problems with wet and dry river beds and the tidal bores in an idealized estuary. The grid convergence of the DG method is conducted in the case of steady state oblique hydraulic jump. For the dam-breaking problem, we investigate the effectiveness of a simple positivity-preserving limiter which is used in the DG method to avoid the non-physical negative water height when the river bed is dry. Finally, we simulate the tidal bores with a trumpet-like shape river mouth similar to the one at the Qiantang River, China and study the effects of the tidal range and river topography, which are related to the propagation and breaking of the undular tidal bores.

3.1. Oblique hydraulic jump

In this simple example with an exact solution, an oblique hydraulic jump is introduced by means of an interaction between a supercritical flow and a converging wall deflected to the left by an angle θ . In the left figure of Fig. 1, a 40m long river with upstream width 30m which is deflected at the location $(x, y) = (10m, 0m)$ by an angle $\theta = 8.95^\circ$ is shown. The initial conditions are $h = 1m, u = 8.57m/s$ and $v = 0m/s$. A free-stream inflow and outflow boundary condition is set for the left and right boundaries respectively. A reflective boundary condition is imposed along the y -direction. It is a classical discontinuous flow problem and often used to validate the accuracy of a numerical algorithm. According to the results in [30,31], the exact steady state solutions are $h = 1.5m, u = 7.956m/s$ and the angle of the hydraulic jump is $\alpha = 30^\circ$.

Assuming the mesh size to be $\tau_K = 0.5m$, we generate the unstructured triangular meshes with the total number of elements $N = 10,586$. A small section of the meshes is shown in the middle figure of Fig. 1. The contour of the water surface level $h + b$ at time $t = 6s$ is shown in the right figure of Fig. 1. The solution reaches the steady state solution and agrees well with those given in the literature [30,31]. Table 1 shows the grid convergence of the numerical solutions which also agree well with the exact solution [32]. The error decays with the decreasing mesh sizes τ_K .

3.2. Dam-breaking problem

Next, we investigate the performance of the positivity-preserving well-balanced DG method in simulating the two-dimensional dam-breaking problems with wet and dry river beds.

² <http://www.dinma.univ.trieste.it/nirftc/research/easymesh/>

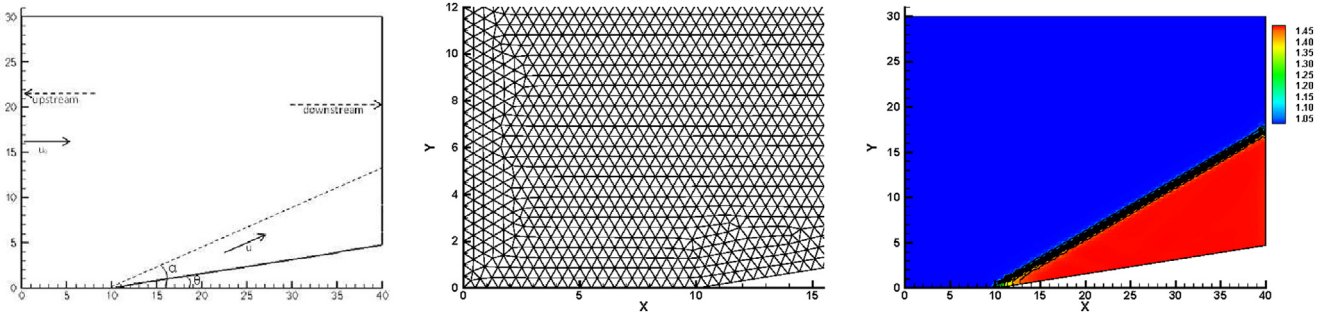


Fig. 1. (Left) The sketch of the computational domain, (Middle) a small section of the meshes and (Right) the water surface level $h + b$ at time $t = 6s$.

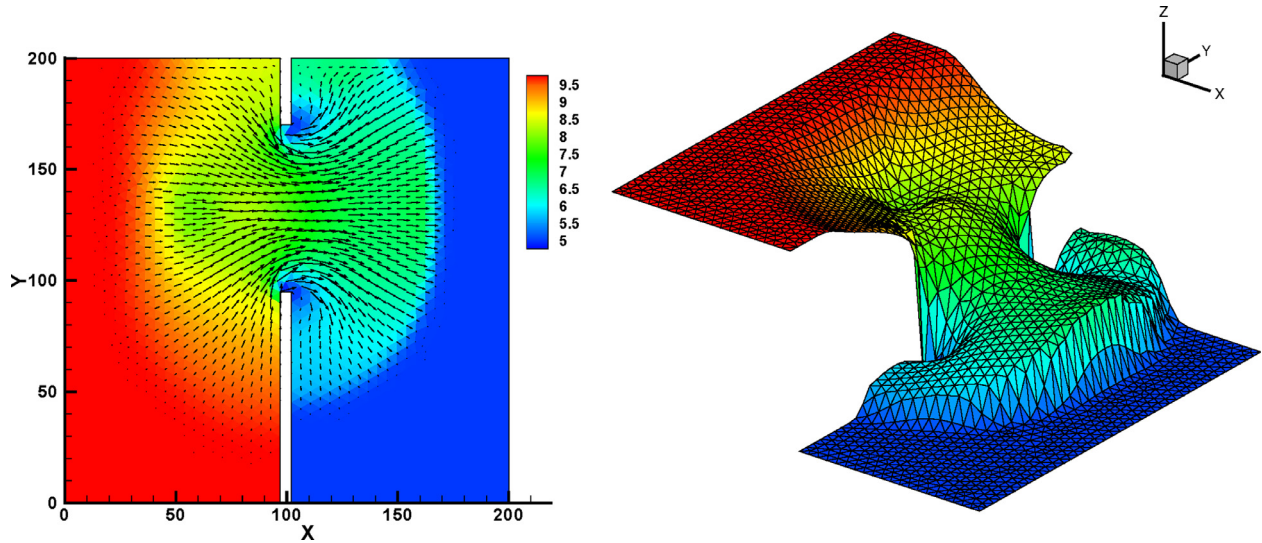


Fig. 2. The dam-breaking problem with a wet river bed. (Left) The contour of the water surface level $h + b$ and its velocity field and (right) the surface of the water surface level $h + b$ at time $t = 7.2$.

The computational domain is $[0, 200]^2$. The width of the dam is set to be 5 and the breach is located from $x = 97$ to $x = 102$ and between $y = 95$ and $y = 170$. A mesh size of $\tau_K = 5$ and $N = 3742$ unstructured triangular elements are generated. The boundary conditions are reflective at the top and bottom boundaries. The inflow and outflow boundary conditions are imposed in the left and right boundaries respectively. The initial conditions are given as

$$h(x, y, 0) = \begin{cases} 10, & \text{if } x \leq 100 \\ h_0, & \text{otherwise} \end{cases}, \quad u(x, y, 0) = v(x, y, 0) = 0, \tag{14}$$

where h_0 is the water height in the river bed.

- For the wet river bed with $h_0 = 5$, the water surface level and its velocity field are shown in Fig. 2 at time $t = 7.2$. The sharp water front formed by the breaking of the dam is captured essentially oscillations free. The shear vortical structures generated at the edges of the breach are similar to those shown in [33] and are well captured by the DG method.
- For the dry river bed with $h_0 = 0$, the water surface level and its velocity field are shown in Fig. 3 at time $t = 7.2$. The results are drastically different from those given in the case with a wet river bed above. For example, there is no vortical rollup structure around the edge of the breach of the dam. The positivity-preserving limiter in the DG method prevents the non-physical negative water height, that is, $h(x, y, t) \geq 0$ at all time. We

observe that the wave front is more gradual, and the two-dimensional flow features in the dry case are less than those in the wet case, which are also consistent with the published results in [34,35].

In this study, we also run the simulations until the final time $t = 50$ in order to examine the long time behaviors of the positivity-preserving well-balanced DG method. In these cases, the computational domain is enlarged to $[0, 600] \times [0, 200]$. Fig. 4 shows the contour lines of the water surface level $h + b$ with both wet and dry river beds at times $t = 10, 20, 50$.

- For the wet river bed (see the left figure of Fig. 4), a strong hydraulic jump (a strong gradient of the water surface in front of flood) is formed at the early time $t = 10$. At time $t = 20$, the hydraulic jump spreads and surges forward, and near the top of breach two vortical rollups due to the shear of the flows are formed. At time $t = 50$, the hydraulic jump maintains its form and moves downstream away from the dam while the vortical rollups are dissipated gradually.
- For the dry river bed (see the right figure of Fig. 4), the flood water rushes out from the breach, but there is no hydraulic jump as that in the wet river bed case. The flood water simply collides with the top wall and a strong reflected wave is formed at time $t = 20$. A similar reflective phenomenon happens on the bottom wall at the later time $t = 50$. During the propagation of the water in the dry river bed, no hydraulic jump in the water

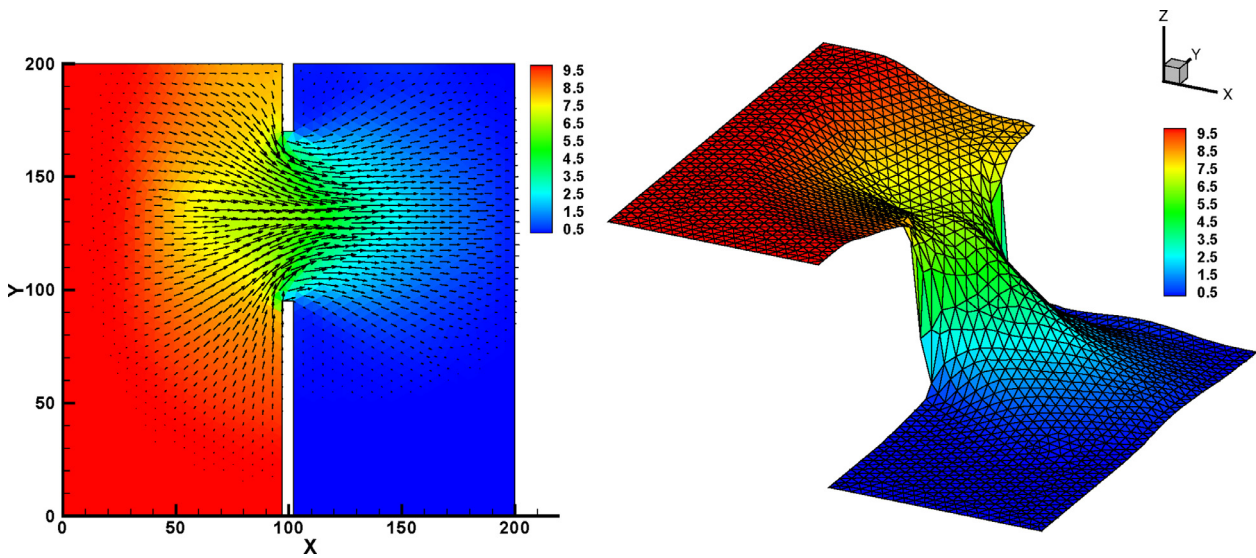


Fig. 3. The dam-breaking problem with a dry river bed. (Left) The contour of the water surface level $h + b$ and its velocity field and (right) the surface of the water surface level $h + b$ at time $t = 7.2$.

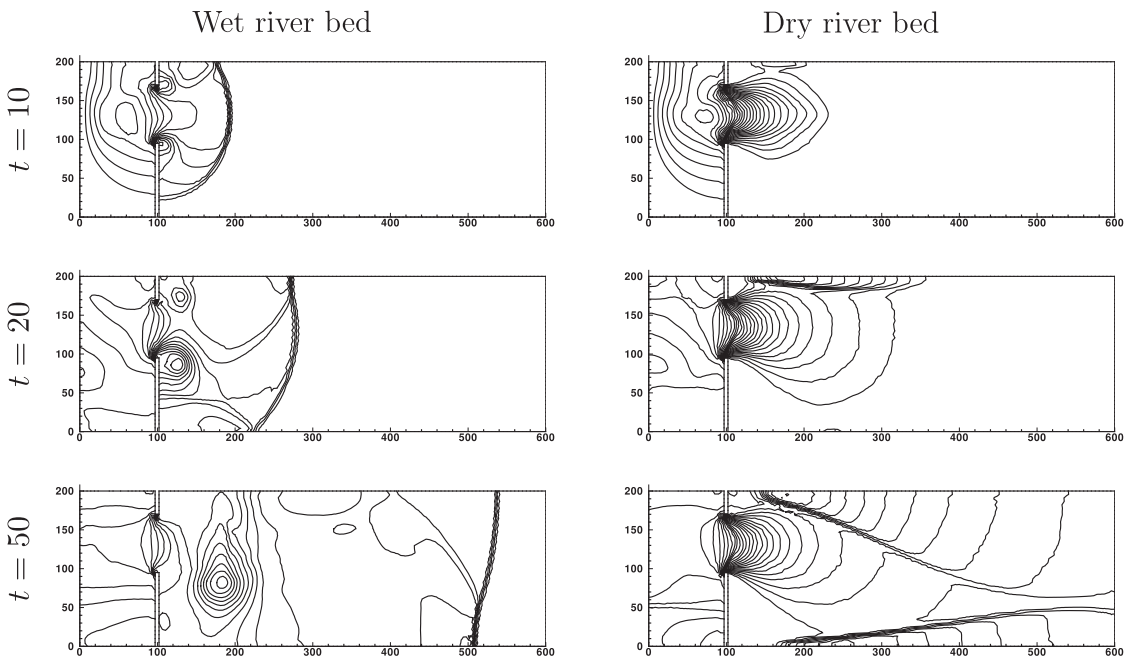


Fig. 4. The contour lines of the water surface level $h + b$ with (left) wet and (right) dry river beds at times $t = 10, 20, 50$.

surface is formed in front of flood because there is no water preventing the flooding of the dry area.

3.3. Tidal bores in an idealized estuary

Along the Qiantang River in Hangzhou, China, with its trumpet shaped mouth, there is the site of the world's largest tidal bores. The tidal bores with waves as tall as 9m move as fast as 40km/h up into the river from the coast. The tide behind the wave makes the river's water rise for hours after the tidal bores pass. The tidal wave sweeps past Hangzhou, menacing ship and destroying docks in the harbor and sweeping unsuspected people off the river bank into the water and drown. In Fig. 5, the temporal evolution of the tidal bores obtained from a measurement of the water height during the period of October 9th–17th, 2010 at a measuring

station Yanguan along the Qiantang River [36] is shown. The sharp steepening of the waves can be observed in the tidal bores.

In this preliminary study, we consider an idealized estuary model similar to the Qiantang River in order to simulate the development and evolution of the large scale gross structures of the tidal bores (see Remark 2). Fig. 6 shows the sketch of an idealized estuary model. For the examples presented below, we take the length of the river to be 900km ($x \in [-900km, 0km]$) in order to avoid spurious waves reflected from the left artificial boundary of a truncated physical domain in a long time simulation. The downstream length of the idealized estuary area is set to be $x \in [0km, 100km]$ in a shape of a trumpet. The angle between the coastline and the river bank line is set to be $\theta = 30^\circ$. The width of the river is set to be $y \in [-2km, 2km]$. The inflow flow rate (flux) of the river at $x = -900km$ is set to be $2000m^3/s$. The river and ocean water surface heights are $h = 10m$ at the initial time $t = 0$ in the whole

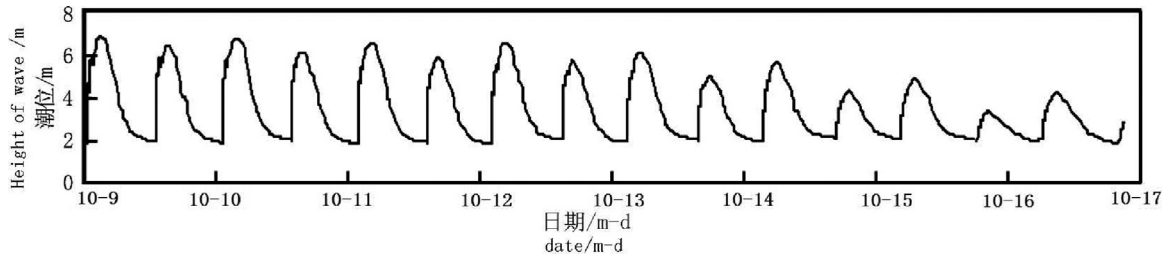


Fig. 5. The temporal evolution of the water height of the tidal bores taken from October 9th–17th, 2010 at a measuring station Yanguan along the Qiantang River, China.

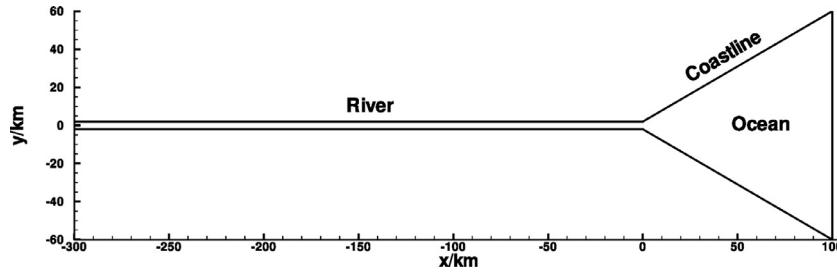


Fig. 6. The sketch of an idealized estuary model.

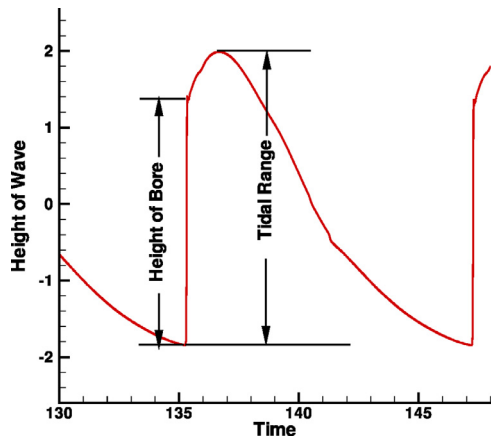


Fig. 7. The illustration of the tidal range and the height of a tidal bore.

estuary system. To simulate the left-going ocean tidal waves in the idealized estuary model, a time dependent sinusoidal perturbation of the water height at the right boundary ($x = 100\text{km}$) is imposed as $h(100\text{km}, t) = a \cos 2\pi\omega t$, where a and $\omega = 1/21600\text{s}^{-1}$ (or $1/12\text{h}^{-1}$) are the incoming tidal wave amplitude and frequency respectively. In the examples below, a mesh size of $\tau_K = 1\text{km}$ and $N = 23,936$ unstructured triangular elements are generated. For the sake of clarity, we define the height of a tidal bore and the tidal range as illustrated in Fig. 7.

We begin by investigating the effect of the incoming tidal wave amplitudes $a = 2\text{m}$ and $a = 1\text{m}$ on the formation of the tidal bores under the idealized estuary system with a flat bottom, that is, $b = 0$.

The left and right figures of Fig. 8 shows the water surface level $h + b$ at six locations $x = 60\text{km}, 10\text{km}, -40\text{km}, -140\text{km}, -200\text{km}, -300\text{km}$ (the positive and negative signs mean that the measurement is taken in the ocean and river side of the idealized estuary system respectively) with the amplitudes $a = 2\text{m}$ and $a = 1\text{m}$ respectively. In the figures, the distances between two dashed lines are 10m and 5m for the amplitudes $a = 2\text{m}$ and $a = 1\text{m}$ respectively.

Table 2

The tidal range and height of the tidal bores at different locations with the amplitudes $a = 2\text{m}$ and $a = 1\text{m}$ in a flat bottom idealized estuary system ($b = 0$).

	Location (km)	60	10	-40	-140	-200	-300
$a = 2\text{m}$	Tidal range (m)	7.4	8.4	7.4	6.6	6.4	5.9
	Tidal height (m)	-	-	6.2	5.9	6.4	5.9
$a = 1\text{m}$	Tidal range (m)	3.5	4.1	3.9	3.8	3.8	3.5
	Tidal height (m)	-	-	-	2.3	3.2	3.1

As the tidal waves move upstream from the right boundary and before entering the river in the trumpet shape region, one can observe 1) the deformation of the shape of the sinusoidal waves, 2) the rising of the water surface level $h + b$, and 3) a shorter wavelength between two tidal waves. More specifically, the wavelengths have changed from $5.5h$ to $4.1h$ at the locations $x = 60\text{km}$ and $x = 10\text{km}$ respectively. It is because the ocean water is funneled into the smaller volume as they move upstream toward the narrowed mouth of the river. The shape was deformed due to the strong nonlinearity of the shallow water equations with large amplitudes. In the case of the smaller amplitude $a = 1\text{m}$, the original sinusoidal shape of the ocean tidal wave is maintained quite well even at the entrance of the narrowed mouth of the river. In either case, the tidal bores have not been fully developed yet.

As the tidal waves continuing to surge up into the river, the strong nonlinearity of the shallow water equations begins to deform the shape of the smooth undular tidal bores further, and to develop a steep gradient in the front of and level off in the back of a tidal bore, for example, at about $x = -40\text{km}$ with $a = 2\text{m}$ and $x = -140\text{km}$ with $a = 1\text{m}$. For the large amplitude $a = 2\text{m}$, the tidal bores heighten and steepen up quickly and reach the maximum local tidal range about 7.4m as the tidal bores move upstream against the water current. For the small amplitude $a = 1\text{m}$, the weaker nonlinearity of the equations allows the smooth undular tidal bores to move further upstream before steepening at around $x = -200\text{km}$ and $x = -300\text{km}$. In Table 2, we show the tidal range and tidal height of the tidal bores in the flat bottom idealized estuary system $b = 0$ with the amplitudes $a = 2\text{m}$ and $a = 1\text{m}$.

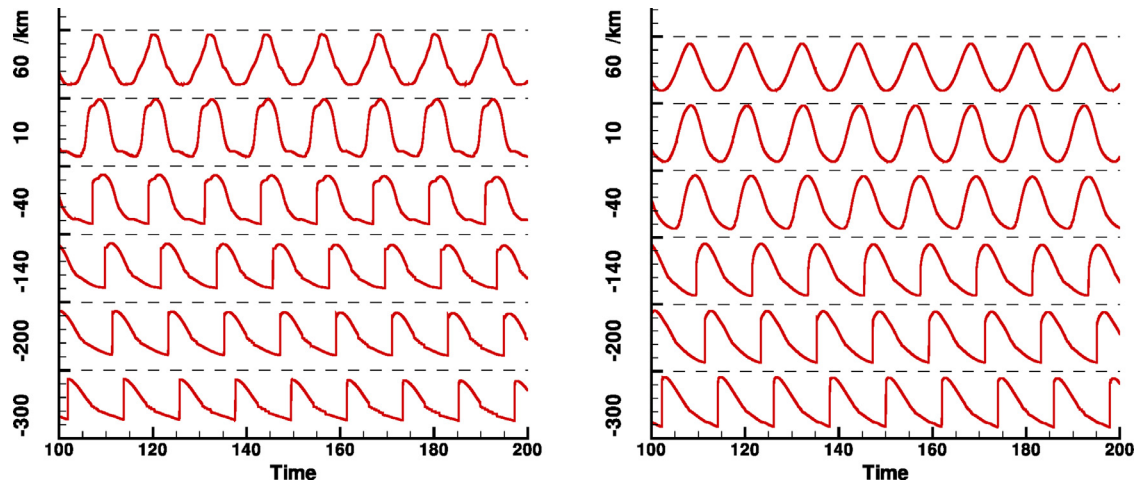


Fig. 8. The evolution of the water surface level $h + b$ of the tidal bores in a flat bottom idealized estuary system ($b = 0$) at different locations with the amplitudes (Left) $a = 2m$ and (Right) $a = 1m$.

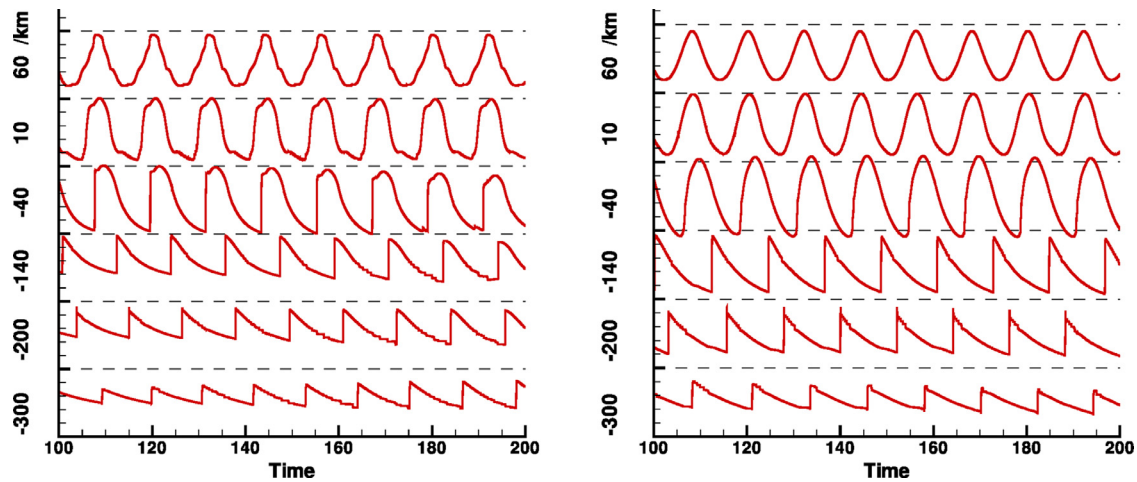


Fig. 9. The evolution of the water surface level $h + b$ of the tidal bores in a non-flat bottom idealized estuary system ($b \neq 0$) at different locations with the amplitudes (left) $a = 2m$ and (right) $a = 1m$.

To demonstrate that the well-balanced DG method performs well with a non-flat bottom $b \neq 0$ in the tidal bore simulations, we also consider the formation and evolution of the tidal bores with a sloped terrain along the mouth of the river, given by

$$b(x, y) = \begin{cases} 0, & \text{if } 0 < x \leq 100 \\ k(x - c) + d, & \text{if } c < x \leq 0 \\ d, & \text{otherwise} \end{cases}, \quad (15)$$

where $c = -300$, $d = 5$, $k = \frac{5}{3} \times 10^{-3}$. The evolution of the water surface level $h + b$ of the tidal bores in a non-flat bottom idealized estuary system ($b \neq 0$) at different locations with the amplitudes $a = 2m$ and $a = 1m$ are shown in Fig. 9. The undular tidal bores are pushed upward sharply and deformed as they move upstream along the river in response to the sloped terrain. The hydraulic jump in the tidal bores appears quicker and closer to the mouth of the river. Moreover, due to the smaller water height h in the river, the hydraulic jumps become smaller as they move upstream in the river at the later time as compared with the flat bottom river above (see Fig. 8).

Remark 2. After the development of the steep tidal bores, strictly speaking, the shallow water equations are no longer a valid formulation in modeling the breaking of the tidal bores and turbulence mixing of the air and water at the tips of the steep front. However,

the equations can still provide some gross observations of the evolution of the tidal bores at the later time.

4. Conclusion and future work

In this work, the positivity-preserving well-balanced DG method on the unstructured triangular meshes was employed to simulate several applications in the computational hydrology, including the oblique hydraulic jump problem, the dam-breaking problem involving wet and dry river beds, and the tidal bores in an idealized estuary model. We verified the accuracy of the proposed DG method using the exact steady state solution of the oblique hydraulic jump, and show that the positivity-preserving limiter worked well in the simulations of dam-breaking problem with a dry river bed. Different flow structures have been observed in the evolution of the flooding in the dam-breaking problem with the wet and dry river beds. At the end, the proposed method is used to simulate the tidal bores in an idealized estuary model, to study the formation and evolution of the tidal bores with a trumpet-like shape river mouth emptying into an ocean while subjected to the large tidal wave inflow, similar to the one at the Qiantang River, China. Numerical examples show that the tidal range and topography of the river bed play an important role in the formation and evolution of the tidal bores.

Other important factors, such as the friction along the river bottom, river topology, sand dune, full moon, shape and size of the estuary and men-made structures (dam, bridges etc.), can greatly affect the formation and evolution of the tidal bores. They will be reported in our on-going research work in the future.

Acknowledgments

The authors would like to acknowledge the funding support of this research by National Natural Science Foundation of China (11201441), Natural Science Foundation of Shandong Province (ZR2012AQ003) and Fundamental Research Funds for the Central Universities (201362033). The author (Don) also likes to thank the Ocean University of China for providing the startup fund (201412003) that is used to support this work. The research of Xing is partially sponsored by NSF grant DMS-1216454. The authors also would like to acknowledge the Third Summer Workshop on Advanced Research in Applied Mathematics and Scientific Computing 2015 at Ocean University of China as a major part of the research was conducted during the workshop.

References

- [1] Bale DS, LeVeque RJ, Mitran S, Rossmannith JA. A wave propagation method for conservation laws and balance laws with spatially varying flux functions. *SIAM J Sci Comput* 2002;24:955–78.
- [2] Bermudez A, Vazquez ME. Upwind methods for hyperbolic conservation laws with source terms. *Comput Fluids* 1994;23:1049–71.
- [3] LeVeque RJ. Balancing source terms and flux gradients on high-resolution Godunov methods: the quasi-steady wave propagation algorithm. *J Comput Phys* 1998;146:346–65.
- [4] Noelle S, Xing Y, Shu C-W. High-order well-balanced schemes. Numerical methods for relaxation systems and balance equations. Russo G, Puppo G, editors. Italy: Seconda Università di Napoli, Quaderni di Matematica, Dipartimento di Matematica; 2009.
- [5] Perthame B, Simeoni C. A kinetic scheme for the Saint-Venant system with a source term. *Calcolo* 2001;38:201–31.
- [6] Xing Y, Shu C-W. High order finite difference WENO schemes with the exact conservation property for the shallow water equations. *J Comput Phys* 2005;208:206–27.
- [7] Berthon C, Marche F. A positive preserving high order VF-Roe scheme for shallow water equations: a class of relaxation schemes. *SIAM J Sci Comput* 2008;30:2587–612.
- [8] Bollermann A, Noelle S, Medvidová ML-. Finite volume evolution Galerkin methods for the shallow water equations with dry beds. *Commun Comput Phys* 2010;10:371–404.
- [9] Brufau P, Vázquez-Cendón ME, G-Navarro P. A numerical model for the flooding and drying of irregular domains. *Int J Numer Methods Fluids* 2002;39:247–75.
- [10] Bunya S, Kubatko EJ, Westerink JJ, Dawson C. A wetting and drying treatment for the Runge–Kutta discontinuous Galerkin solution to the shallow water equations. *Methods Appl Mech Eng* 2009;198:1548–62.
- [11] Gallardo JM, Parés C, Castro M. On a well-balanced high-order finite volume scheme for shallow water equations with topography and dry areas. *J Comput Phys* 2007;227:574–601.
- [12] Audusse E, Bouchut F, Brisseau MO, Klein R, Perthame B. A fast and stable well-balanced scheme with hydrostatic reconstruction for shallow water flows. *SIAM J Sci Comput* 2004;25:2050–65.
- [13] Kurganov A, Levy D. Central-upwind schemes for the Saint-Venant system. *Math Model Numer Anal* 2002;36:397–425.
- [14] Bryson S, Epshteyn Y, Kurganov A, Petrova G. Well-balanced positivity preserving central-upwind scheme on triangular grids for the Saint-Venant system. *ESAIM Math Model Numer Anal* 2011;45:423–46.
- [15] Ern A, Piperno S, Djadel K. A well-balanced Runge–Kutta discontinuous Galerkin method for the shallow-water equations with flooding and drying. *Int J Numer Methods Fluids* 2008;58:1–25.
- [16] Xing Y, Zhang X, Shu C-W. Positivity-preserving high order well-balanced discontinuous Galerkin methods for the shallow water equations. *Adv Water Resour* 2010;33:1476–93.
- [17] Xing Y, Zhang X. Positivity-preserving well-balanced discontinuous Galerkin methods for the shallow water equations on unstructured triangular meshes. *J Sci Comput* 2013;57:19–41.
- [18] Xing Y, Shu C-W. A survey of high order schemes for the shallow water equations. *J Math Study* 2014;47:221–49.
- [19] Cockburn B, Karniadakis GE, Shu C-W. The development of discontinuous Galerkin methods. In: Cockburn B, Karniadakis G, Shu C-W, editors. *Discontinuous Galerkin methods: theory, computation and applications. Lecture notes in computational science and engineering, part I: overview, vol. 11.* New York: Springer; 2000. p. 5–50.
- [20] Schwanenberg D, Königeter J. A discontinuous Galerkin method for the shallow water equations with source terms. In: Cockburn B, Karniadakis G, Shu C-W, editors. *Discontinuous Galerkin methods: theory, computation and applications. Lecture notes in computational science and engineering, part I: overview, vol. 11.* Berlin: Springer; 2000. p. 289–309.
- [21] Dawson C, Proft J. Discontinuous and coupled continuous/discontinuous Galerkin methods for the shallow water equations. *Comput Methods Appl Mech Eng* 2002;191:4721–46.
- [22] Eskilsson C, Sherwin SJ. A triangular spectral/hp discontinuous Galerkin method for modelling 2d shallow water equations. *Int J Numer Methods Fluids* 2004;45:605–23.
- [23] Giraldo FX, Hesthaven JS, Warburton T. Nodal high-order discontinuous Galerkin methods for the spherical shallow water equations. *J Comput Phys* 2002;181:499–525.
- [24] Nair RD, Thomas SJ, Loft RD. A discontinuous Galerkin global shallow water model. *Mon Weather Rev* 2005;133:876–88.
- [25] Kesserwani G, Liang Q. Well-balanced RKDG2 solutions to the shallow water equations over irregular domains with wetting and drying. *Comput Fluids* 2010;39:2040–50.
- [26] Rhebergen S, Bokhove O, van der Vegt JJW. Discontinuous Galerkin finite element methods for hyperbolic nonconservative partial differential equations. *J Comput Phys* 2008;227:1887–922.
- [27] Xing Y, Shu C-W. A new approach of high order well-balanced finite volume WENO schemes and discontinuous Galerkin methods for a class of hyperbolic systems with source terms. *Commun Comput Phys* 2006;1:100–34.
- [28] Zhang X, Shu C-W. On maximum-principle-satisfying high order schemes for scalar conservation laws. *J Comput Phys* 2010;229:3091–120.
- [29] Cockburn B, Lin SY, Shu C-W. TVB Runge–Kutta local projection discontinuous Galerkin finite element method for conservation laws III: one-dimensional systems. *J Comput Phys* 1989;84:90–113.
- [30] Alcrudo F, Garcia-Navarro P. A high-resolution Godunov-type scheme in finite volumes for the 2d shallow water equations. *Int J Numer Methods Fluids* 1993;16:489–505.
- [31] Henderson FM. *Open channel flow.* New York: Macmillan; 1996.
- [32] Wang JW, Liu RX. A comparative study of finite volume methods on unstructured meshes for simulation of 2d shallow water wave problems. *Math Comput Simulat* 2000;53:171–84.
- [33] Anastasiou K, Chan CT. Solution of the 2d shallow water equations using the finite volume method on unstructured triangular meshes. *Int J Numer Methods Fluid* 1997;24:1225–45.
- [34] Baghlani A. Simulation of dam-break problem by a robust flux-vector splitting approach in cartesian grid. *Sci Iran* 2011;18:1061–8.
- [35] Liang D, Lin B, Falconer RA. Simulation of rapidly varying flow using an efficient TVD-maccormack scheme. *Int J Numer Methods Fluids* 2007;53:811–26.
- [36] Xie D, Pan C, Lu B, Ye X. A study on the hydrodynamic characteristics of the qingtang tidal bore based on field data. *China J Hydro* 2012;27:501–8.